WPPFC-CPR(18) 18769

L Vignitchouk et al.

# Survival and in-vessel redistribution of disruption-induced beryllium droplets in ITER

Preprint of Paper to be submitted for publication in Proceeding of 23rd International Conference on Plasma Surface Interactions in Controlled Fusion Devices (PSI-23)

This work has been carried out within the framework of the EUROfusion Consortium and has received funding from the Euratom research and training programme 2014-2018 under grant agreement No 633053. The views and opinions expressed herein do not necessarily reflect those of the European Commission.

# Accumulation of newly generated beryllium dust in ITER diagnostic ports after off-normal events

L. Vignitchouk[a,*], S. Ratynskaia[a], P. Tolias[a], R.A. Pitts[b], G. De Temmerman[b], M. Lehnen[b], D. Kiramov[c,d]

[a] *Space and Plasma Physics, KTH Royal Institute of Technology, SE-100 44 Stockholm, Sweden*
[b] *ITER Organization, Route de Vinon-sur-Verdon, CS 90 046, 13067 St-Paul-lez-Durance, France*
[c] *Kurchatov Institute, Moscow 123182, Russian Federation*
[d] *National Research Nuclear University MEPhI, Moscow 115409, Russian Federation*

**Abstract**

Dust transport simulations are used to predict the effect of diagnostic ports on the spatial distribution of solid beryllium particles in ITER after mitigated disruptions. Beryllium dust is assumed to originate from the partial vaporization and subsequent re-solidification of liquid droplets initially ejected during first-wall transient melting events. The trajectories of droplets launched with various initial conditions, as well as the time evolution of their temperature and mass, are simulated until either complete vaporization or immobilization upon undergoing a sticking or splashing impact with the wall is realized. The results indicate that approximately 10% of the dust mass in the vessel can be expected to reside inside ports, in particular those located in the equatorial plane or in the lower outboard first wall.

*Keywords:* beryllium, dust, droplets, disruptions

## 1. Introduction

Metallic dust particles are routinely produced in fusion devices as a result of a variety of plasma-wall interaction processes. In ITER, the amount of in-vessel mobilizable dust is restricted to 1000 kg by the nuclear licensing agreement, with much more stringent limits imposed to dust lying on hot plasma-facing components owing to the risk of explosion caused by dust-steam chemical reactions in case of accidental water leakage in the vessel [1–4]. Currently, the main dust creation mechanism foreseen in ITER involves the ejection and subsequent re-solidification of liquid beryllium (Be) droplets from molten layers induced by high-energy transients [4], similarly to a process which has been observed experimentally for Be JET [5] and molybdenum in Alcator C-Mod [6].

Recently, the first predictive study addressing the possible outcomes of such droplet ejection events was conducted with the MIGRAINe dust dynamics code [7]. The key findings of this work concern the low conversion rate of liquid droplets into solid dust and the emergence of the divertor legs and lower outboard first wall regions as preferential accumulation sites for the surviving dust. The purpose of the work presented here is to extend the analysis of the MIGRAINe simulations reported in [7] by focusing on Be particles susceptible to penetrate into port openings in the first wall. In fact, ports can be considered as effective dust sinks, which may remove a fraction of the in-vessel dust from plasma-facing components, and in particular hot surfaces. Moreover, potential dust accumulation in the vicinity of the outer divertor baffle may impede the operation of the in-vessel viewing system (IVVS), designed to carry out a variety of diagnostic tasks between discharges [8].

## 2. Method

The results presented in this paper rely on MIGRAINe simulations which have been described extensively in [7]. Here, we repeat only the key aspects of the simulation layout and focus on how the presence of diagnostic ports can be accounted for in the analysis.

### *2.1. Simulation parameters and physical model*

Similarly to all fusion-relevant dust transport codes [9], MIGRAINe simulates the evolution of single spherical conducting grains under the action of particle, heat and momentum fluxes in a prescribed plasma background [10]. Here, two main scenarios are considered, corresponding to a major disruption (MD) and an upward vertical displacement event (VDE), both with delayed mitigation by massive neon injection during the current quench. DINA simulations [11] of these disruptions provide the required time-varying plasma density and temperature, as well as the evolution of its spatial boundary (see figures 1 and 2 in [7]).

*Corresponding author
*Email address:* ladislas.vignitchouk@ee.kth.se
(L. Vignitchouk)

Be droplets are launched over a 3 ms period following the thermal quench from the first wall locations expected to receive the strongest plasma heat flux, as shown in figure 1. In the VDE scenario, this corresponds to the plasma-wall contact point; in the MD scenario, three injection points have been selected from field-line tracing. The initial droplet radius and velocity are varied in the ranges 10–150 $\mu$m and 0.1–200 m s$^{-1}$, respectively, covering the representative values reported in theoretical and experimental studies of droplet ejection from molten metallic layers under plasma exposure (see e.g. [12–15]).

While immersed in the plasma, the coupled evolution of the droplets' mass, bulk temperature and floating potential is determined according to the model presented in [16], which includes thin sheath effects on ion collection and strong magnetization effects on electron collection. The presence of multiply charged mitigating neon ions and their effect on droplet heating — in particular through the release of their stored ionization energy upon neutralization at the droplet surface — is also accounted for; a detailed analysis of the relative contribution of each charging and heating process can be found in table 2 of [7]. Outside the plasma, surviving droplets cool down and possibly re-solidify via thermal radiation and heat exchange with the surrounding neon-deuterium gas mixture.

The ion drag force, which typically governs the dynamics of small dust particles in steady-state plasmas [9] was shown to have a relatively small impact in the scenarios of interest here, due to the large initial droplet sizes and speeds [7]. It was ignored in the simulations and dust/droplet motion reduces to free-falling parabolic arcs, both inside and outside the plasma. The outcome of collisions between the simulated Be particles and the wall is determined as follows: if the impinging particle is still in the liquid state, the collision is treated as sticking and a liquid splash is assumed to form at the impact location; if the particle is in the solid state, the Thornton and Ning collision model [17] is employed as in [10] to predict whether the incident velocity is large enough for the dust grain to rebound and how much of its kinetic energy is dissipated during the impact. The wall geometry implemented in the simulations is toroidally symmetric and does not include diagnostic ports.

### *2.2. Output analysis*

For each set of initial conditions, the simulated trajectory terminates upon satisfying one of three conditions: (i) complete vaporization inside the plasma, (ii) splashing impact upon colliding with the wall while in the liquid state, (iii) sticking impact upon colliding with the wall while in the solid state and with an incident velocity below the sticking threshold. For those particles able to exit the plasma (conditions (ii) and (iii)), the MIGRAINe output consists of the particle state (time, position, velocity, mass, radius and temperature) at its termination point, as well as at each intermediate bouncing point.

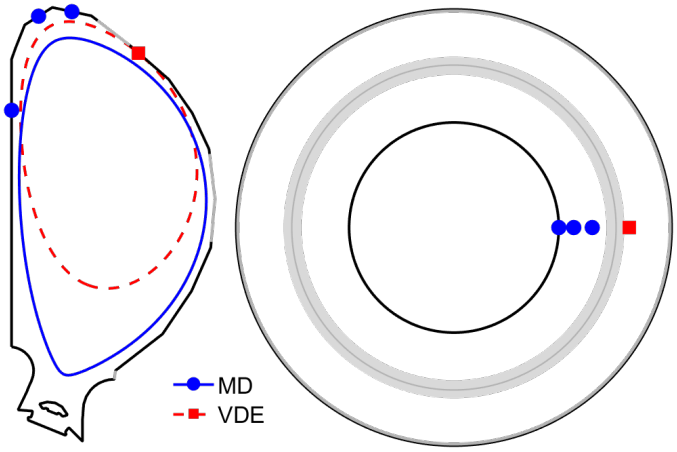


Figure 1: Poloidal and toroidal ITER cross-sections used in the simulations, showing the three toroidally symmetric ports in gray. The droplet injection locations and the boundary of the thermal quench plasma in both scenarios are indicated. See [7] for more details on the evolution of the plasma parameters.

While the results presented in [7] rely exclusively on the final particle state, information on intermediate bounces can be used to account for the presence of diagnostic ports as perfectly absorbing wall elements: it suffices to check whether bounces occurred at a port location. If so, the corresponding particle is considered to enter the port and its final state is overwritten by the relevant intermediate state. Since droplet trajectories are tracked in three dimensions, this method allows for the inclusion of toroidally asymmetric features. However, as discussed in section 3.1, in order to maintain sufficient statistics, we shall consider three toroidally symmetric ports as shown in figure 1, namely an upper port, an equatorial port, and an IVVS port located between the outer divertor baffle and the lower outboard first wall.

As in [7], final quantities of interest such as the fraction of initially injected Be mass converted into solid dust are computed by assigning statistical weights to single-trajectory results according to chosen distributions of the droplet injection parameters. Here, the initial droplet velocity is assumed to follow a uniform, isotropic distribution over the 0.1–200 m s$^{-1}$ speed range and all possible injection angles. The initial droplet radius is assumed to follow one of three upper-limit log-normal (ULLN) distributions [18], with modal value 30 $\mu$m ("small" sizes), 75 $\mu$m ("medium" sizes), or 120 $\mu$m ("large" sizes).

## 3. Results and discussion

Accounting for the presence of diagnostic ports via the post-treatment method described in 2.2 can only affect particles whose trajectories feature at least one bouncing impact. For this reason, all results that pertain to droplets which completely vaporize or splash on the wall while still liquid are unchanged from [7]. *In all the following, we focus exclusively on solid Be dust entering any of the ports.*

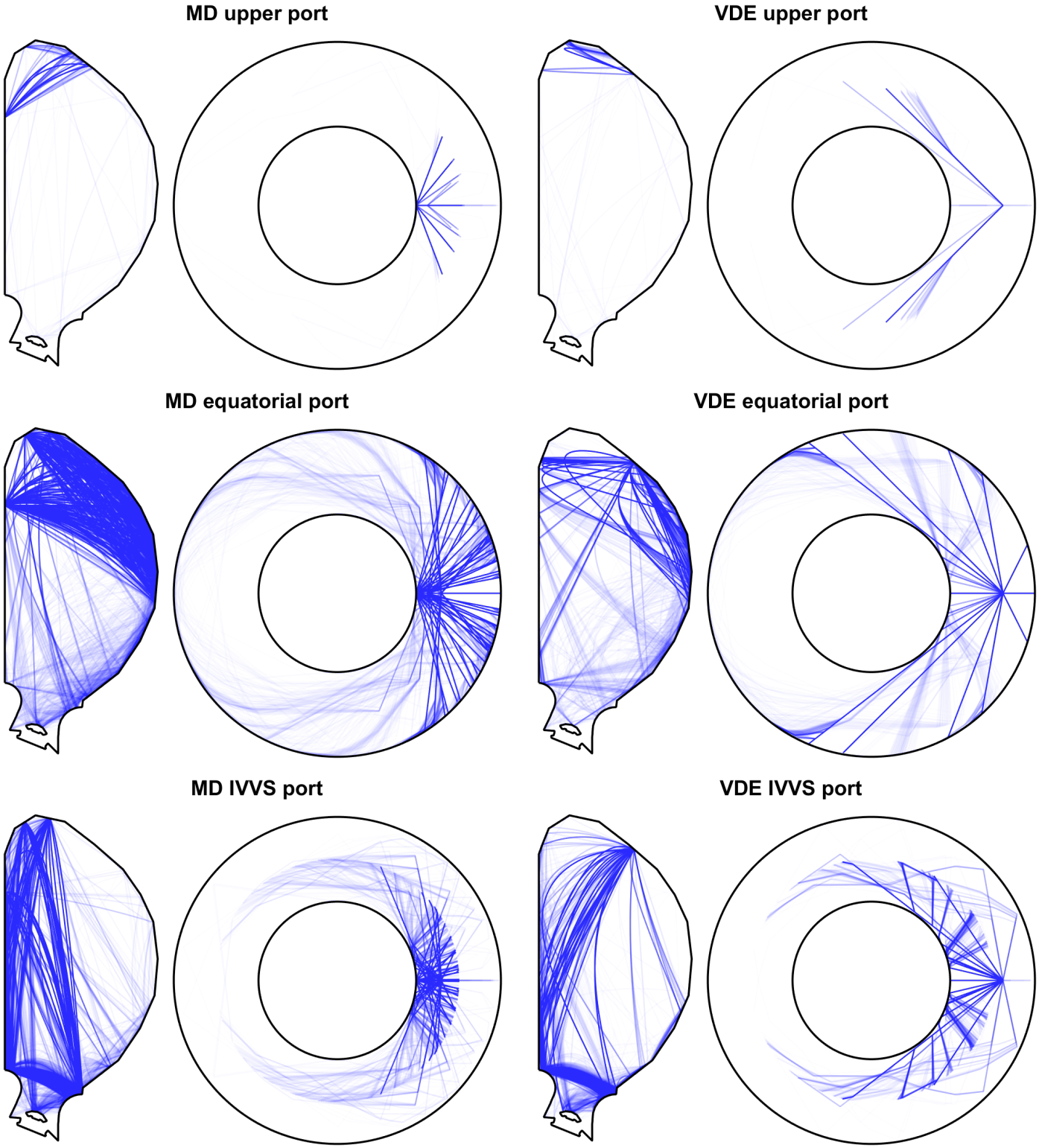


Figure 2: Simulated trajectories of re-solidifying droplets entering the ports. Each curve is plotted with low opacity so that color saturation reflects the trajectory density, i.e. which droplet injection velocities are more strongly represented.

### 3.1. Preferred trajectories of dust entering ports

Even though the size of the diagnostic ports is overestimated in the simulations due to the toroidal symmetry assumption, entering a port remains a relatively rare occurrence, as indicated by the trajectory sample sizes given in table 1. More details can be found in figure 2, which shows the trajectories of re-solidifying particles terminating into each port, thereby providing information on which droplet injection velocities are favoured.

Overall, the equatorial port emerges as the most efficient dust sink, as could be expected from its large area. However, the clear differences that can be observed between the trajectories entering each port cannot be explained by area alone. This is due to importance of bouncing impacts, which have a considerable effect on the velocities of the particles moving in the plasma chamber. Whereas the equatorial and IVVS ports can be reached after multiple bounces on the wall, the upper port is almost entirely populated by particles launched directly towards it. This represents less than 1% of the simulated trajectories due to the small solid angle it subtends with respect to the droplet injection points. On the contrary, the IVVS port appears to be ideally located to receive particles that rebound on the inner divertor baffle or the dome. As a result, the trapping efficiency of IVVS port greatly exceeds the value expected from its area alone, as detailed in table 1.

Figure 2 also illustrates the resolution of the droplet injection angle scan in the simulations, which is insufficient to obtain meaningful quantitative results on the dependence of the dust deposition pattern with respect to the toroidal angle. This is partly due to the fact that, for a given injection angle, the initial speed and size do not drastically affect the particle's path, rather its survival, its time of flight, and whether it is allowed to undergo bouncing collisions. This is especially visible on the toroidal projections of figure 2, where the trajectories appear grouped in sheaves, which get progressively spread out at each collision with the wall.

### 3.2. Dust size and mass distributions

Table 2 details the mass distribution of dust particles in the diagnostic ports with different distributions of the initial droplet size. These results are in general agreement with those of section 3.1, namely that the equatorial and IVVS ports collect a comparable quantity of Be dust, of the order of 5% of the total in-vessel dust mass, despite their difference in area. The fact that dust can accumulate in the small IVVS port also agrees with the results of [7], where it was shown that the lower outboard region of the plasma chamber was a preferential dust deposition site.

The characteristic sizes of the particles residing in diagnostic ports are found to be representative of the total dust population in the vessel. This is exemplified by figure 3, where it can be seen that the statistical dust radius distributions in each port share the same qualitative features as the global distribution, namely a marked peak close to 3 $\mu$m, corresponding to droplets which barely escaped complete vaporization by the plasma, and a more uniform spread over larger sizes.

## 4. Conclusions

The effect of diagnostic ports on the spatial distribution of beryllium dust in the ITER vessel after disruptions was investigated. By identifying and selecting the preferred particle trajectories leading to deposition in the ports, approximately 10% of the dust mass in the vessel is expected to be deposited in the ports, while the remaining 90% tends to accumulate in the divertor legs or under the dome. The results also show that the efficiency of the ports as a sink for dust particles depends not only on the port area, but also on its poloidal location. In particular, the in-vessel viewing system port is shown to be able to collect a large number of particles bouncing on the inner divertor baffle or on the dome. The size distribution of dust particles residing inside the ports is also found to be similar to that of the total in-vessel dust population, which suggests that small dust samples collected locally may be used for global diagnostic purposes, provided that there is no preferred droplet ejection angle, as assumed in the simulations.

Although the main conclusions of [7] on the identification of the divertor region as the principal dust accumulation site are essentially unchanged, particles residing in the ports are much less likely to be mobilized by subsequent plasma exposures, implying that their relative contribution to the in-vessel dust inventory may be larger on the long term. Further work is required to provide a quantitative comparison between the expected mobilization/erosion and re-deposition rates over the course of several discharges. In particular, the response of beryllium dust adhered on the divertor plates to normal plasma conditions emerges as the next research topic of interest.

## Acknowledgments

ITER is the Nuclear Facility INB no. 174. This paper applies new physics analysis to the estimation of potential dust production in ITER due to high energy transients which is not yet incorporated into the ITER technical baseline. The nuclear operator is not constrained by the results presented here. The views and opinions expressed herein do not necessarily reflect those of the ITER Organization. This work has been carried out within the framework of the EUROfusion Consortium (WPPFC) and has received funding from the Euratom research and training programme 2014–2018 under grant agreement No 633053. The views and opinions expressed herein do not necessarily reflect those of the European Commission. S.R. and P.T. would also like to acknowledge the financial support of the Swedish Research Council.

| | Upper port | Equatorial port | IVVS port | Total |
|---|---|---|---|---|
| MD | 1082 (0.7%) | 14421 (9.5%) | 7907 (5.2%) | 152070 |
| VDE | 279 (0.4%) | 3855 (5.0%) | 3617 (4.7%) | 77791 |
| Area ratio | 4.0% | 11.7% | 0.9% | |

Table 1: Trajectory sample sizes used to construct statistical distributions of solid Be dust in the ports. The last column indicates the total sample size for solidified particles. The percentages in brackets represent the number fraction of the total sample size, to be compared with the ratios of the port area to the total wall area on the last line.

| | MD | | | VDE | | |
|---|---|---|---|---|---|---|
| | Small | Medium | Large | Small | Medium | Large |
| Modal droplet radius [$\mu$m] | 30 | 75 | 120 | 30 | 75 | 120 |
| Global dust mass fraction [%] | 3.3 | 2.0 | 1.0 | 0.6 | 1.1 | 0.7 |
| Upper port dust mass fraction [%] | 0.8 | 0.2 | 0.01 | 0.9 | 0.6 | 0.1 |
| Equatorial port dust mass fraction [%] | 11.7 | 5.7 | 2.8 | 7.4 | 5.8 | 6.5 |
| IVVS port dust mass fraction [%] | 4.2 | 4.0 | 3.7 | 3.3 | 4.3 | 4.0 |

Table 2: Mass fraction of the solid dust residing in the diagnostic ports. The global dust mass fraction is given with respect to the initial droplet mass, dust mass fractions in the ports are given with respect to the global dust mass fraction.

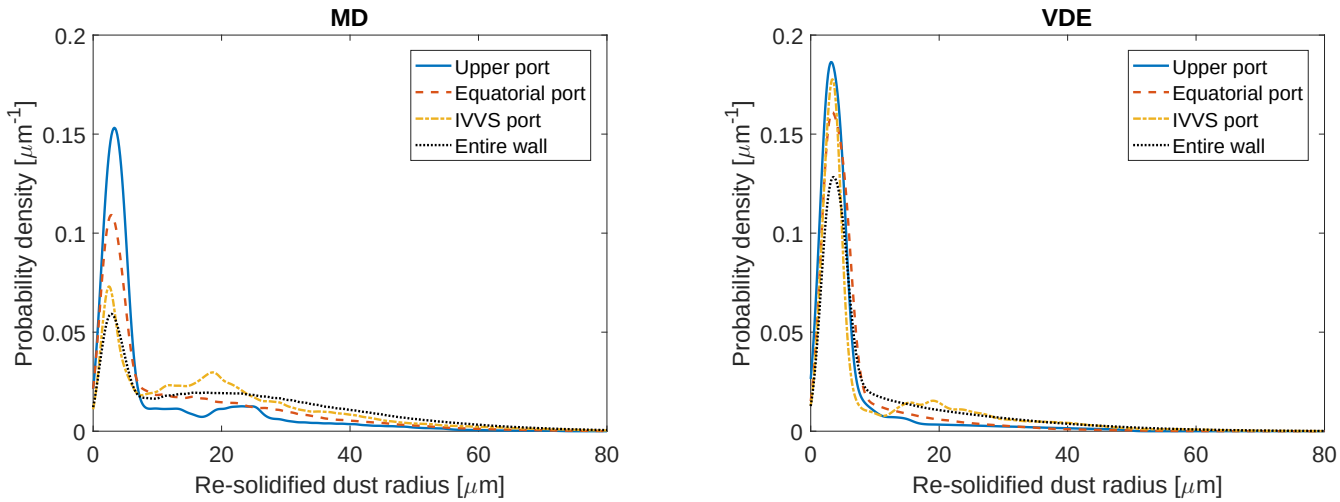


Figure 3: Comparison between the size distribution of solid dust residing in ports and the size distribution of the total in-vessel dust, for initial droplet injection conditions for droplet injection following the uniform velocity distribution and the small-size upper-limit log-normal size distribution (30 $\mu$m modal droplet radius).

## References


[1] S. Rosanvallon, C. Grisolia, P. Andrew, et al., J. Nucl. Mater. 390–391 (2009) 57.

[2] N. Taylor, D. Baker, V. Barabash, et al., Fusion Sci. Technol. 56 (2009) 573.

[3] N. Taylor, C. Alejaldre, P. Cortes, Fusion Sci. Technol. 64 (2013) 111.

[4] M. Shimada, R. A. Pitts, S. Ciattaglia, et al., J. Nucl. Mater. 438 (2013) S996.

[5] J. C. Flanagan, M. Sertoli, M. Bacharis, et al., Plasma Phys. Control. Fusion 57 (2015) 014037.

[6] C. Arnas, J. Irby, S. Celli, et al., Nucl. Mater. Energy 11 (2017) 12.

[7] L. Vignitchouk, S. Ratynskaia, P. Tolias, et al., Nucl. Fusion 58 (2018) 076008.

[8] N. Casal, P. Bates, O. Bede, et al., Fusion Eng. Des. 96–97 (2015) 742.

[9] S. I. Krasheninnikov, R. D. Smirnov, D. L. Rudakov, Plasma Phys. Control. Fusion 53 (2011) 083001.

[10] L. Vignitchouk, P. Tolias, S. Ratynskaia, Plasma Phys. Control. Fusion 56 (2014) 095005.

[11] R. R. Khayrutdinov, V. E. Lukash, J. Comput. Phys. 109 (1993) 193.

[12] B. Bazylev, G. Janeschitz, I. Landman, et al., Fusion Eng. Des. 84 (2009) 441.

[13] S. Pestchanyi, I. Garkusha, V. Makhlaj, I. Landman, Phys. Scripta T145 (2011) 014062.

[14] A. V. Arzhannikov, V. A. Bataev, I. A. Bataev, et al., J. Nucl. Mater. 438 (2013) S677.

[15] A. Baron-Wiechec, E. Fortuna-Zaleśna, J. Grzonka, et al., Nucl. Fusion 55 (2015) 113033.

[16] L. Vignitchouk, S. Ratynskaia, P. Tolias, Plasma Phys. Control. Fusion 59 (2017) 104002.

[17] C. Thornton, Z. Ning, Powder Technol. 99 (1998) 154.

[18] B. Bazylev, I. Landman, A. Loarte, et al., Phys. Scr. T138 (2009) 014061.